Fission-Track Thermochronology in Structural Geology and Tectonic Studies

11

David A. Foster

Abstract

Apatite fission-track (AFT) and zircon fission-track (ZFT) data along with other low-temperature thermochronologic data are widely used in the fields of structural geology and tectonics to determine the timing/duration of events, the amount of exhumation in mountain belts, rates of slip on faults, and the geometries of fault networks. In this chapter, I review applications of AFT and ZFT data in extensional tectonic settings. Examples of data sets and interpretations are summarized from the Cenozoic-Recent North American Basin and Range Province. These data constrain displacements of normal faults, rates of slip on faults, paleogeothermal gradients, and the original dip of low-angle normal faults.

11.1 Introduction

Fission-track (FT) data on apatite and zircon (AFT and ZFT, respectively) are important tools for structural geology and tectonics, as was recognized from the earliest studies in mountain belts (Wagner and Reimer 1972). These low-temperature thermochronometers have been widely used to constrain the magnitude and timing of faulting in the brittle upper crust through displaced age–elevation profiles, and the rates of displacement of crust being exhumed through closure temperature (T_c) isotherms by faulting and erosion. The direct application of FT thermochronology in structural geology is more common for extensional or transtensional tectonic settings where cooling is a result of "tectonic" exhumation along with erosion (e.g., Fitzgerald et al. 1991; Foster et al. 1991). There are, however, many excellent examples of FT data being applied to thrust and fold belt systems (e.g., O'Sullivan et al. 1993; McQuarrie et al. 2008; Espurt et al. 2011; Mora et al. 2014) to determine when particular thrusts or thrust systems were active. When thrusting forms topographic relief and induces rapid erosion and cooling, the FT data constrain the timing of thrusting (e.g., Metcalf et al. 2009). The delay in time between thrusting and erosion in some orogenic belts, however, limits direct measurement of fault parameters from cooling ages in many shortening systems. This chapter is, therefore, focused on examples from rifts, fault blocks, and metamorphic core complexes, particularly in environments where tectonic exhumation usually dominates over erosion.

11.2 Faulted Partial Annealing Zone (PAZ) Profiles to Constrain Fault Geometry

In regions lacking traditional sedimentary or volcanic stratigraphic markers, geologic structure and fault block geometry may be constrained using relative displacements of a reference AFT or ZFT age/track length relief profile, if regional consistency in the profile is established (e.g., Gleadow and Fitzgerald 1987; Brown 1991; Fitzgerald 1992; Foster and Gleadow 1992; Foster et al. 1993; Stockli et al. 2003). Reference profiles are constructed by measuring FT ages and track lengths from samples collected over a wide range of elevations in steep mountainous terrain or from drill holes. Paleo-PAZ inflection(s) in the FT age–elevation profile and steep gradients in the reference profile reveal the upper crustal thermal history of an area (e.g., Foster and Gleadow 1993) and form the basis for a pseudo-stratigraphy (Brown 1991) (see also Chap. 10, Malusà and Fitzgerald 2018a, b). Vertical offsets in the reference profile are due to normal faulting and block tilting that has occurred after the PAZ profile was formed in an originally stable region. An AFT age and mean track length stratigraphy can be viewed as being composed of layers of crust with similar (to within ±10–20 °C) thermal histories

D. A. Foster (✉)
Department of Geological Sciences, University of Florida, Gainesville, FL 32611, USA
e-mail: dafoster@ufl.edu

M. G. Malusà and P. G. Fitzgerald (eds.), *Fission-Track Thermochronology and its Application to Geology*,
Springer Textbooks in Earth Sciences, Geography and Environment, https://doi.org/10.1007/978-3-319-89421-8_11

for temperatures below ~100–120 °C prior to faulting (Brown 1991). Vertical offsets between reference age–elevation profiles that are beyond two-sigma errors are used to constrain displacements on faults; sample traverses perpendicular to structural trends may elucidate block tilting and horizontal displacement. This approach is generally able to detect faults with displacements of the order of hundreds of meters or more and is most applicable to regions that had been geologically stable and slowly eroded for timescales of $>10^7$ year prior to extension (Brown et al. 1994). A comprehensive review of AFT PAZ profiles is given in Chap. 9, (Fitzgerald and Malusà 2018).

11.3 Kenya and Anza Rifts Example of Fault Geometry

The plot in Fig. 11.1a shows a reference AFT age–elevation profile for basement rocks exposed east and west of the Kenya Rift in central Kenya (Foster and Gleadow 1993, 1996). The reference profile is composed of data from samples collected from steep mountain fronts at intervals of <100 m. The filled boxes are data from the Cherangani Hills, a range west of the Kenya Rift that reaches elevations of >3000 m, and the remaining data are from the Mathews Range and Karisia Hills, which are east of the Kenya Rift (Foster and Gleadow 1996). The samples from the Karisia Hills are elevated 1100 m to reconstruct displacement due to Cenozoic faulting (Foster and Gleadow 1992). The reference profile exhibits three segments where the age–elevation relationship is linear with a rather steep slope (and long track lengths for the lowest segment). These are separated by two preserved PAZ intervals, which were established before periods of more rapid erosion at about 120 Ma and about 65 Ma. A similar age–elevation relationship is found throughout Kenya and Tanzania, establishing the regional nature of the FT stratigraphy (e.g., Foster and Gleadow 1996; Noble et al. 1997; Spiegel et al. 2007; Toores Acosta et al. 2015).

Figure 11.1b shows a plot of the topography along an east–west section at 1˚10′N latitude. The section crosses the Miocene-Recent Kenya Rift and the Cretaceous–Paleogene Anza Rift. The variation in AFT age with elevation in the mountain ranges, and with distance along the traverses between the ranges, is superimposed on the topographic section from the reference stratigraphy in the inset box. The three segments with steep slopes (and consistent mean track lengths), and the two paleo-PAZs in Fig. 11.1a, define five FT stratigraphic markers. Offsets in segments of the reference profile indicate the presence of faults with displacements estimated by restoring the formerly continuous layers. The FT stratigraphy also reveals the tilt direction for the footwall blocks bounded by the normal faults, which in this case is consistent across the section. These data suggest that the normal faults were related to extension that formed the Anza Rift, and that the modern East Africa Rift, in Kenya, is superimposed on structures related to previous rifting. In this example, the AFT stratigraphy reveals the broad structural framework of the basement areas east and west of the Kenya Rift where traditional stratigraphic markers are lacking. It is important to note that the small-scale structure may be significantly more complex than shown in Fig. 11.1b, because the resolution of the FT data reveals only structures with displacements of the order of hundreds of meters.

11.4 Normal Fault Slip Rates

Low-temperature thermochronometers are an effective way to determine the rate of slip on normal faults, which is a key parameter for understanding the development of fault systems, particularly low-angle normal faults bounding metamorphic core complexes (e.g., Foster et al. 1993; John and Foster 1993; Foster and John 1999; Wells et al. 2000; Campbell-Stone et al. 2000; Carter et al. 2004, 2006; Stockli 2005; Brichau et al. 2006; Fitzgerald et al. 2009). Lateral gradients in apparent age along strike in the displacement direction of normal faults are related to the progressive quenching of footwall rocks as they moved through the PAZ (or the partial retention zone—PRZ) for the thermochronometer (Fig. 11.2), as long as the footwall was below (at higher temperature) the base of the PAZ before slip occurred (Foster et al. 2010). The inverse of the slope on a plot of apparent age versus distance in the slip direction reveals the slip rate. For accurate slip rate estimates, the T_c isotherm for the thermochronometer must have remained approximately horizontal or fixed during the interval of slip revealed by the data (Ketcham 1996; Ehlers et al. 2003). This assumption was investigated for low-angle normal faults using 2-D conductive cooling models by Ketcham (1996) and found to be reasonable with a few million years after the onset of extension, because the isotherms reach a steady-state position by that time. Before the first few million years, the isotherms advance along the detachment surface causing uncertainties in the slip rate (Ketcham 1996). Advection of isotherms will result in an underestimate of the slip rate (Ehlers et al. 2001; Fitzgerald et al. 2009). The thermochronometric data alone give time-averaged slip rates on timescales of about a million years and do not rule out significantly faster or slower rates of detachment slip over shorter timescales. Ehlers et al. (2003) showed that combining low-temperature thermochronologic data, along with thermal–kinematic modeling of the evolving isotherms, revealed changes in slip rate on the steeply dipping (45°–60°) Wasatch normal fault.

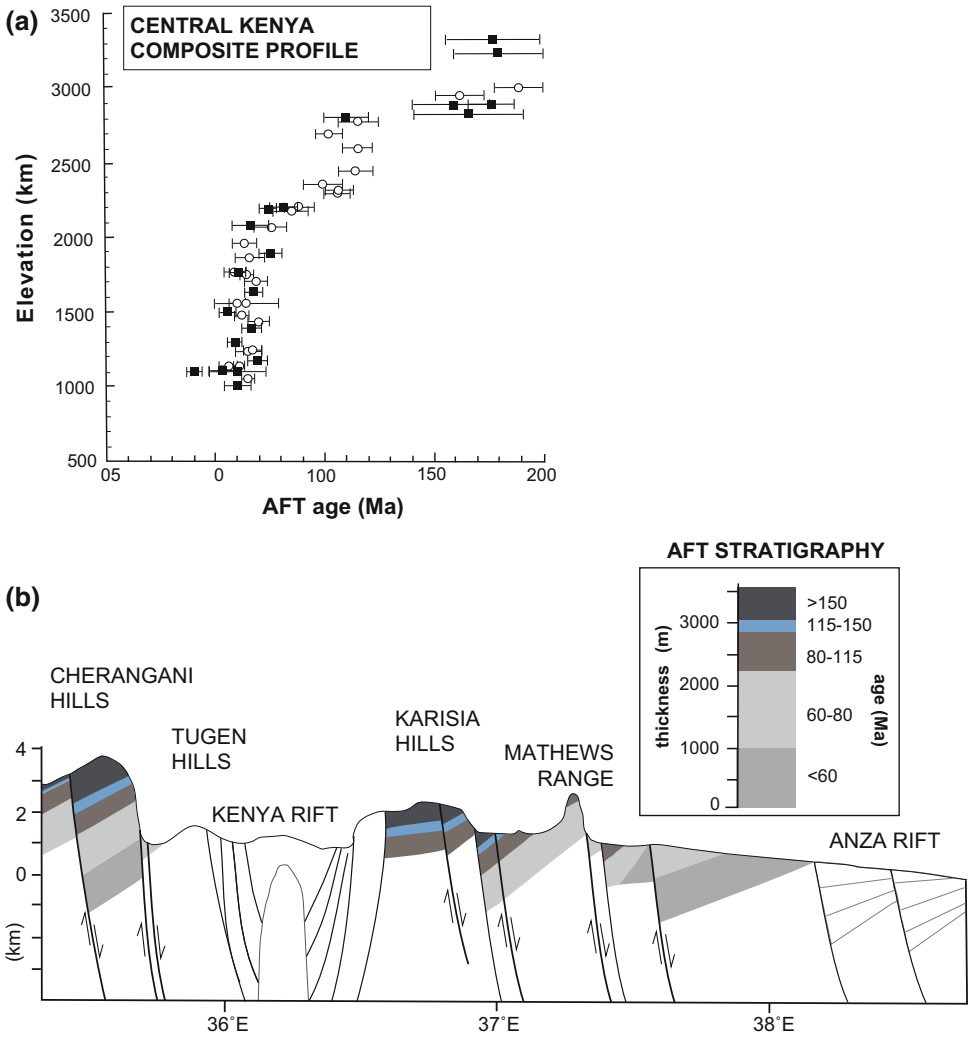

Fig. 11.1 **a** Composite AFT age versus elevation regional profile for central Kenya (after Foster and Gleadow 1996). This age–elevation profile establishes an AFT stratigraphy, which is used to reconstruct offsets on normal faults and constrain tilting of fault blocks. **b** Offsets of the regional AFT age–elevation profile show the gross framework of normal faults that bound the basement mountain ranges in central Kenya (after Foster and Gleadow 1996). Without the FT data, it would not be possible to determine the regional-scale normal faults or block tilting related to the Anza Rift, because no regional sedimentary or volcanic stratigraphy exists within the areas where mainly Precambrian basement rocks are exposed

11.5 Bullard Detachment Example to Constrain Slip Rates

The Bullard detachment is a large-scale, low-angle normal fault that separates footwall rocks of the Miocene Buckskin-Rawhide and Harcuvar metamorphic core complexes in Arizona, USA (Spencer and Reynolds 1991; Scott et al. 1998). Spencer and Reynolds (1991) estimated about 90 km of displacement for this detachment system based on reconstructing distinctive sedimentary and plutonic units in the hanging wall and footwall. Figure 11.3 is a plot of the variation of AFT age with distance in the slip direction for Buckskin-Rawhide and Harcuvar metamorphic core complex footwall rocks, immediately beneath the projection of the detachment (Foster et al. 1993). The inverse slope of the Buckskin-Rawhide core complex data suggests a detachment fault slip rate of 7.7 ± 3.6 km/Myr (±2 sigma). Regressions of the slip rate and two-sigma errors, for these and other slip rates, were calculated using methods of York (1969) for non-correlated errors, considering two-sigma errors in age and sample location/projection. For the regressions of the AFT data, in those cases where the number of data points is relatively small the two-sigma errors are considered to approximate the uncertainties.

All of the samples from the Buckskin-Rawhide footwall give cooling ages at least 5 or 6 million years younger than the onset of extension and have long mean track lengths, indicating rapid cooling. A value of 6.5 ± 3.0 km/Myr for slip rate along that detachment is given by results from the adjacent Harcuvar Mountains core complex. The trend in the Harcuvar Mountains is influenced by one relatively precise AFT age of about 21 Ma from the structurally shallowest sample. Removing this one sample, because of the possibility it may have cooled before the depth of the 110 °C isotherm was stationary (e.g., Ketcham 1996), gives a slip rate of 7.7 ± 3.1 km/Myr. As expected, this rate is similar to that from the Buckskin Mountains because both footwalls were unroofed from beneath the same detachment system (Spencer and Reynolds 1991).

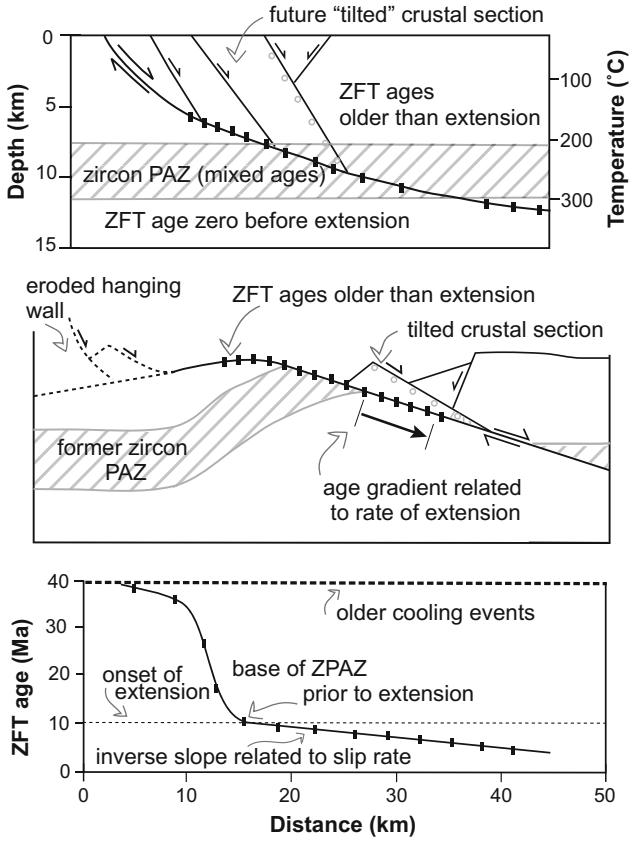

Fig. 11.2 Example showing the exhumation of a zircon PAZ by slip on a low-angle normal fault system (after Foster and John 1999; Wells et al. 2000; Stockli 2005; Foster et al. 2010). The upper diagram shows the zircon PAZ at depth before extension, with the future locations of the normal fault system. The filled boxes represent sample locations above, within, and below the PAZ. The gray circles represent potential sample locations in a future tilted crustal section bounded by normal faults. The middle plot shows the exhumation of the PRZ and crust beneath the zircon PAZ by displacement on a low-angle normal fault. The lower plot shows the distribution of ZFT ages along the trace of the detachment in the direction of slip 10 million years after extension. The samples that were above the zircon PAZ (ZPAZ) reveal cooling ages older than the time of extension, those that were within the ZPAZ give mixed ages that progressively get younger with depth, the samples that were beneath the ZPAZ at deeper depths show a gradual decrease in age with distance, the inverse of which gives the slip rate on the fault. A similar concept also applies to other thermochronologic systems with different PAZ or PRZ temperature intervals

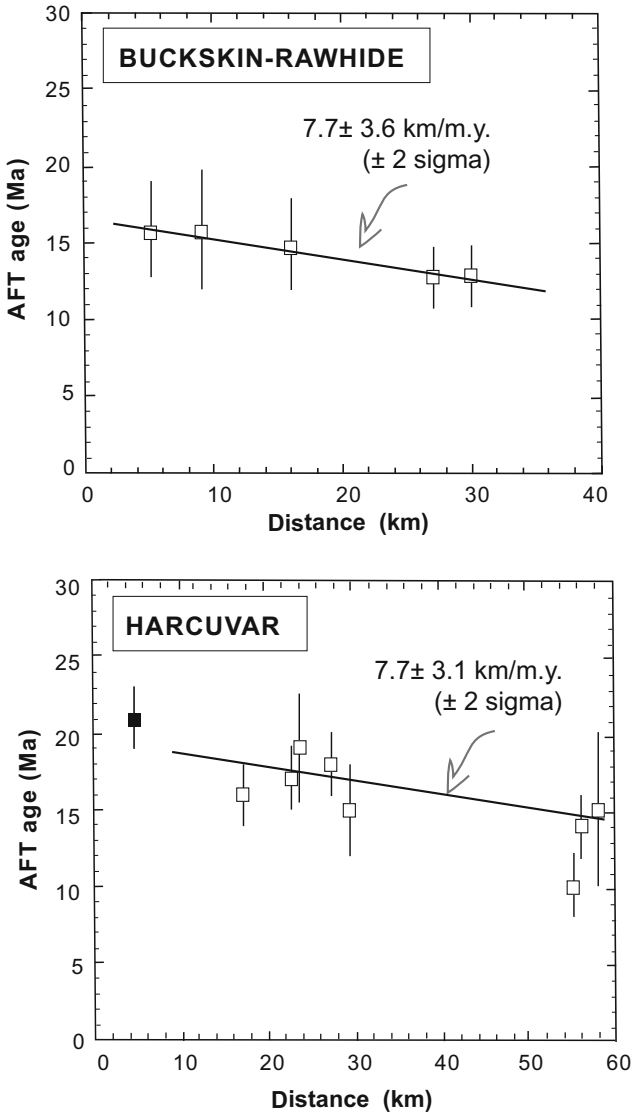

Fig. 11.3 Plots of AFT age against distance in the displacement direction of the Bullard detachment in the Buckskin-Rawhide and Harcuvar metamorphic core complex footwalls

Spencer and Reynolds (1991) independently estimated an extension rate of 8–9 km/Myr along the Buckskin-Rawhide detachment, based on the amount of slip (~90 km) that had occurred between 23 and 25 Ma (when syn-extensional basins started to form) and about 15 Ma (when the lower plate rocks cooled >100 °C). The timing of initial exposure of footwall rocks at the southwestern and northeastern ends of the Buckskin-Rawhide core complex, based on distinctive clasts in conglomerates, also indicates a slip rate of ~7 km/Myr for this fault (Scott et al. 1998).

The relatively large errors for the Miocene AFT ages result in significant two-sigma errors for slip rate examples in Fig. 11.3. Carter et al. (2004) and Singleton et al. (2014) showed that a more precise measurement of slip rate of this fault could be constrained using (U-Th)/He data. Although the results of these two studies are not in agreement on the slip rate (for reasons listed below), they are within error of the values in Fig. 11.3. Displacement rates for other normal faults in the Basin and Range using FT data referenced in this section range from <1 km/Myr to >10 km/Myr.

The example in Fig. 11.3 appears relatively clear with the exception of the relatively large errors. There are notable examples in the literature where AFT and/or other low-temperature thermochronologic data from normal fault

systems are much more complicated and reasonable estimates of slip rate are not possible to constrain. Many detachment faults are composite structures that form from the merger of discrete segments active at different times (e.g., Lister and Davis 1989). This occurs when fault segments are transferred from the footwall to the hanging wall, or from the hanging wall to the footwall, and where secondary breakaway zones develop (e.g., Lister and Davis 1989). Data sets from composite detachments may show overlapping segments or repeated age/distance relationships parallel to the slip direction (e.g., Pease et al. 1999; Campbell-Stone et al. 2000; Stockli et al. 2006; Fitzgerald et al. 2009; Singleton et al. 2014) that need to be assessed separately. Hydrothermal flow within active normal fault systems may result in rapid quenching of the footwall or heating along the detachment (e.g., Morrison and Anderson 1998). The data quality from some detachments is poor due to low uranium concentration, numerous fluid inclusions, and other factors which may mean the slip rate cannot be constrained (e.g., Fitzgerald et al. 1993). Finally, the footwalls of some normal fault systems are too deeply eroded and/or folded by isostatic rebound to project sample locations to the level of the former fault surface (e.g., Foster and Raza 2002).

11.6 Paleogeothermal Gradient

An elusive, but important parameter, for understanding extensional tectonics is the value of the geothermal gradient before extension started. Knowing the geothermal gradient prior to the onset of extension is important for elucidating processes that drive extension in a particular region. Active or passive extension processes, and those driven by magmatism or thermal weakening of the lithosphere, are partly related to different geothermal gradients. Elevated geothermal gradients commonly accompany extension due to mantle upwelling and decompression melting. Gradients prior to extension, however, are often much different and relate to a previous tectonic regime, but are invaluable for calculating the paleodepths of T_c isotherms before exhumation.

There are several examples where FT studies from tilted fault blocks have yielded information about the geothermal gradient prior to extension (Foster et al. 1991; Fitzgerald et al. 1991, 2009; Howard and Foster 1996; Stockli et al. 2003; see also Chap 9, Fitzgerald and Malusà 2018). Paleogeothermal gradient data may then be used to determine, for example, the amount of exhumation that has taken place in metamorphic core complexes and the original dip of faults. Samples collected along traverses from tilted crustal sections (thick fault blocks) parallel to the movement direction of normal faults reveal thermal histories from increasingly deeper paleodepths. Paleoisotherms are identified at the depth where isotopic systems recording pre-extension cooling ages, at shallow depths, give way, at deeper levels, to cooling ages that mark rapid exhumation during extension. The transition where the age–depth curve forms a break-in slope and intersects the age versus paleodepth curve at the time that extension started represents the base of an exhumed PAZ (Fitzgerald et al. 1991; Howard and Foster 1996). A geothermal gradient may be calculated when two paleoisotherms are revealed by thermochronologic data (see Chap. 8, Malusà and Fitzgerald 2018a, b), or one paleoisotherm combined with the location of an unconformity with known depth beneath the surface.

In the Basin and Range Province, examples of this method include studies of the Gold Butte fault block in Utah (Fitzgerald et al. 1991, 2009; Reiners et al. 2000; Bernet 2009; Karlstrom et al. 2010), the Grayback fault block in Arizona (Howard and Foster 1996), and the White Mountains fault block in California/Nevada (Stockli et al. 2003). In each of these cases, the depth below an unconformity (of known depth) for the PAZ for AFT and ZFT (or PRZ for (U-Th)/He ages) is relatively well constrained. The depth of the base of an exhumed PAZ/PRZ relating to the depth of a particular geotherm (e.g., 110° for base of the apatite PAZ) within a relatively intact fault block then allows the calculation of the paleogeothermal gradient.

In the three southern Basin and Range examples listed above, the pre-extension gradients were found to have been relatively low ($\leq$20 °C/km, e.g., Grayback) or normal ($\leq$25 °C/km, Gold Butte). This has important implications for the tectonic setting of the region in Paleogene time. Relatively, normal paleogeothermal gradients indicate that magmatism was unlikely to have weakened the crust prior to extension and even lower geothermal gradients (<20 °C/km) are more typical of subduction zone settings rather than orogenic highlands. In the case of the US Cordillera, the relatively low Paleogene geothermal gradients may be related to cooling of the lithosphere over a flat slab segment of the subducting Farallon Plate (e.g., Dumitru et al. 1991).

11.7 Grayback Fault Block Example to Constrain Paleogeothermal Gradients

The Grayback fault block in the Tortilla Mountains, Arizona (Fig. 11.4), exposes a Proterozoic through Paleocene granitic crustal section about 12-km thick (Howard and Foster 1996). The crustal section was tilted eastward during Oligocene to Miocene extension, which led to the exhumation of core complexes in the Santa Catalina, Rincon, Tortolita, and Picacho Mountains (Dickinson 1991). Stratigraphy of the overlying Tertiary rocks indicates that

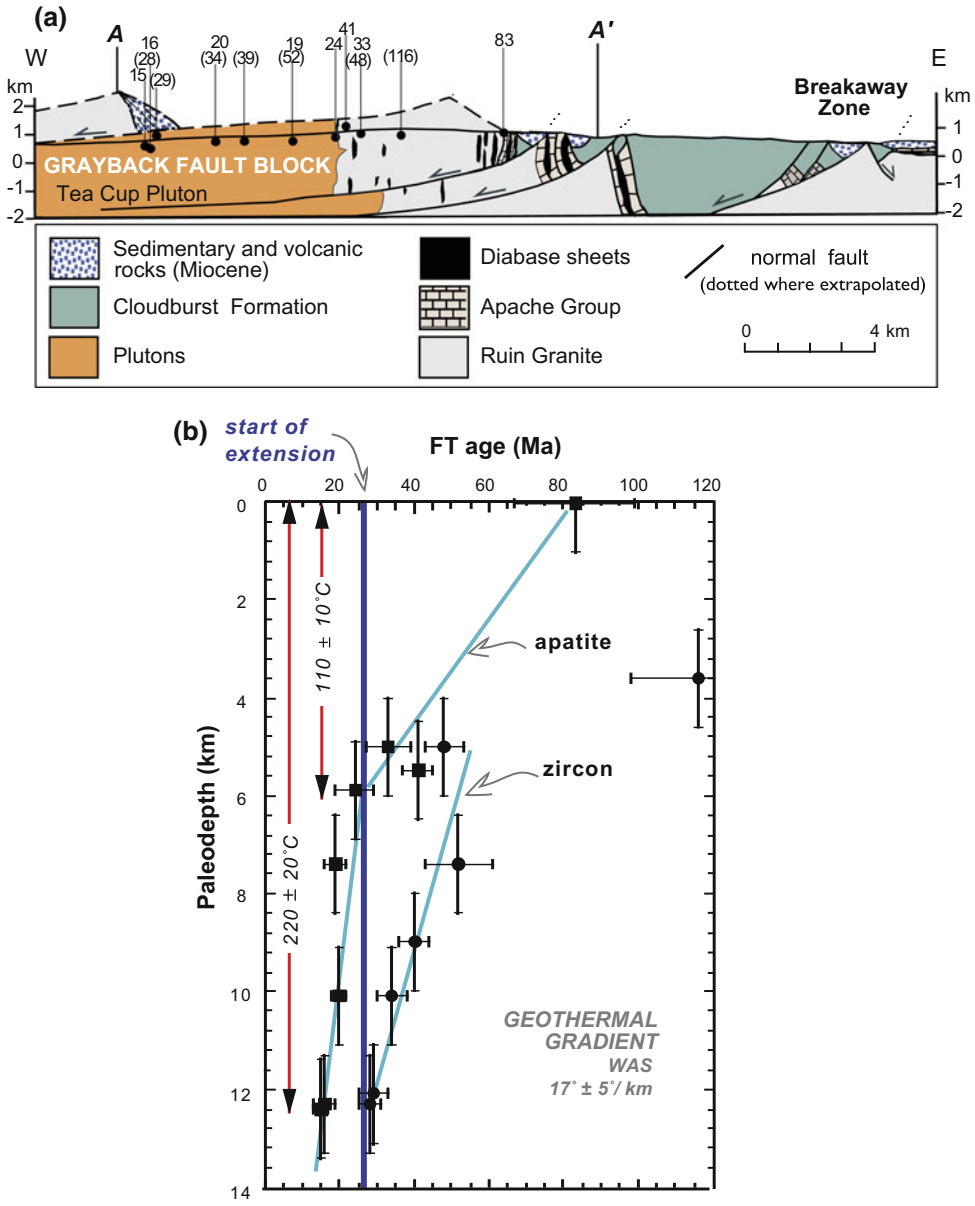

Fig. 11.4 **a** Cross-section of the Grayback fault block in southern Arizona with AFT and ZFT (*italic*) ages (after Howard and Foster 1996). **b** Plot of AFT and ZFT ages against paleodepth for the Grayback block, Arizona (after Howard and Foster 1996)

tilting of the Grayback block took place between 25 and 16 Ma. The block was titled to near-vertical or a slightly overturned orientation based on the dip of Proterozoic Apache Group and diabase dikes that were horizontal prior to tilting (Howard 1991).

AFT and ZFT ages from the Grayback fault block are shown in a plot of age against paleodepth (Fig. 11.4b). The AFT ages decrease westward (deeper paleodepths) from ~83 Ma at the unconformity to a break-in slope at ~24 Ma and ~5–6 km depth. Mean track lengths for samples between 0 and 6 km depth are <13 µm, indicating relatively slow cooling through the apatite PAZ. Below ~5–6 km depth, the AFT ages decrease from ~24–15 Ma and have long mean track lengths (>14 µm), indicating more rapid cooling. The ZFT ages also decrease to the west and become concordant with the initiation of extension at paleodepths of 12.1–12.3 km.

The break-in slope in the AFT age transect represents the position of the base of the apatite PAZ (~110 °C) (Gleadow and Fitzgerald 1987) prior to Tertiary tilting. All of the apatite samples below the break-in slope were cooled rapidly from temperatures where tracks were totally annealed, based on the long mean track lengths. The form of the ZFT age profile with no Oligocene–Miocene break-in slope suggests that all of the samples were at or colder than and structurally above the temperature of total annealing (~220–250 °C for 10^7 year timescales, e.g., Brandon et al. 1998; Bernet 2009). However, the fact that the ages of the two deepest samples

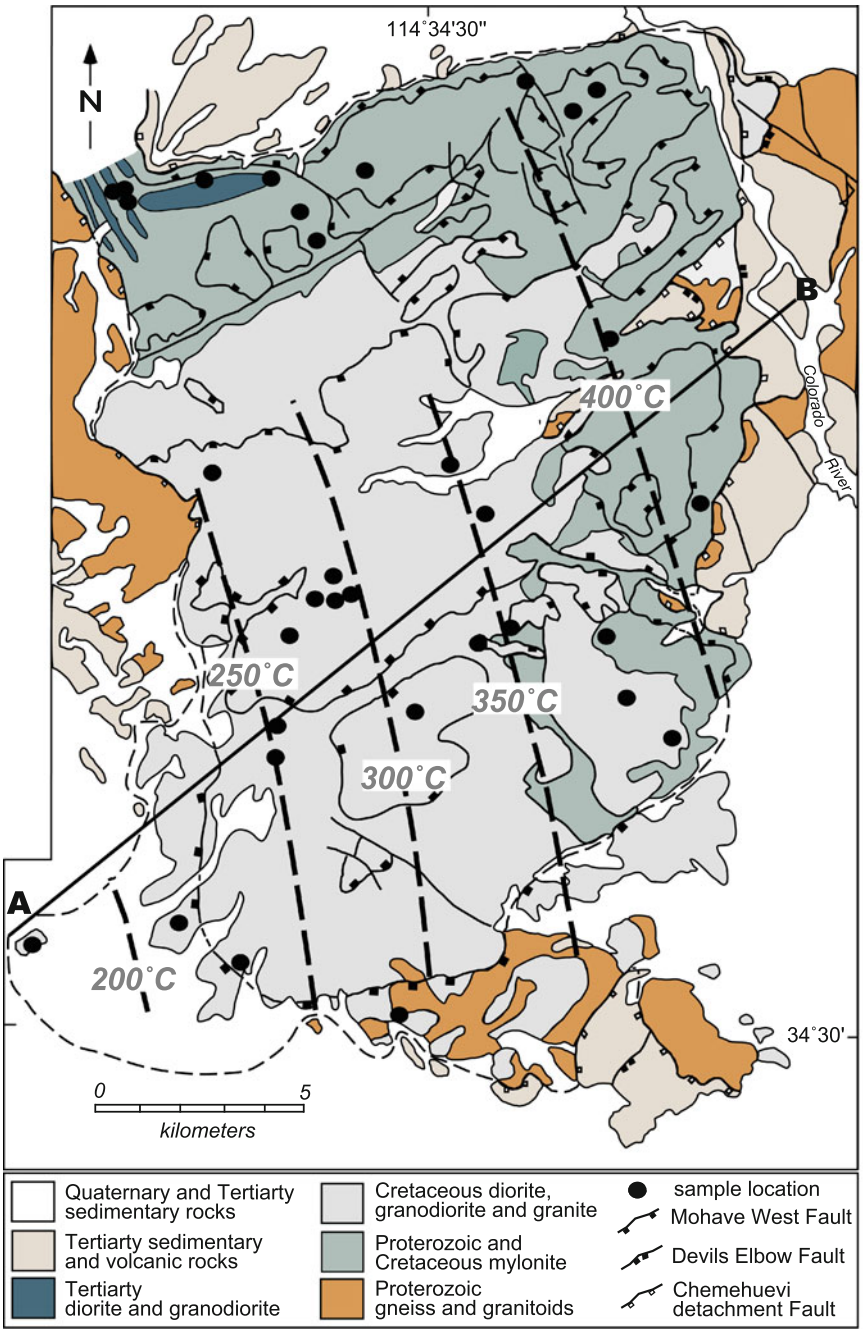

Fig. 11.5 Geological map of the Chemehuevi Mountains, California (modified from John and Foster 1993; Foster and John 1999). The section A–B is the projection through the southern part of the footwall in Fig. 11.6. The thick dashed lines are paleoisotherms for the southern and central parts of the footwall to the Chemehuevi detachment fault when extension started at ~22 Ma. Paleotemperatures for sample points constraining the isotherms were calculated from thermal histories of the footwall rocks obtained from $^{40}Ar/^{39}Ar$ and FT data, where three to five minerals with different T_c were analyzed from each sample. The isotherms show a gradual increase in temperature to the northeast in the known direction of tectonic transport. Isotherms are not shown for the northern part of the footwall, because of syn-extensional plutons in that area

are concordant with, but not younger than, start of tilting suggests the samples at 12.3 km were at 220 ± 30 °C at ~25 Ma.

Howard and Foster (1996) calculated the paleogeothermal gradient for the Grayback block from the difference in depth of the paleoisotherms at 5.7 ± 0.4 km (110 ± 10 °C) and 12.15 ± 0.7 km (220 ± 30 °C). This gives a gradient of 17.1 ± 5.3 °C/km. The errors include values of known and estimated errors in annealing temperatures and the projections. A gradient calculated between the surface and

the 110 ± 10 °C isotherm, assuming a surface temperature of 15 ± 10 °C for the late Oligocene, gives a gradient of 16.7 ± 4.9 °C/km. The mean of these two estimates gives a paleogeothermal gradient of 17 ± 5 °C/km.

11.8 Dip Angles of Faults Prior to Tilting and Isostatic Rebound

One of the fundamental parameters in structural reconstructions of normal and detachment fault systems is the dip of normal faults, when they were initiated and while they are active. This information is essential for calculating extensional strain on local and regional scales and is needed to assess models for the formation of low-angle detachment faults in the light of apparent contradictions with Andersonian fault mechanics (e.g., John and Foster 1993; Wernicke 1995). Tilting of fault blocks and isostatic rebound commonly reduces the dip of faults during and after displacement (e.g., Wernicke and Axen 1988; Spenser and Reynolds 1991). Reconstructing the original dips of faults that do not intersect or offset stratigraphic or other geometric indicators in crystalline rocks is particularly difficult. The controversy regarding the original dips of low-angle detachment faults through the seismogenic crust serves as an example of how difficult it is at times to reconstruct extensional fault systems. Thermochronology data, including FT data, have contributed greatly to the understanding of normal fault systems and initial dips of faults (e.g., Foster et al. 1990; John and Foster 1993; Lee 1995; Foster and John 1999; Pease et al. 1999; Stockli 2005; Fitzgerald et al. 2009).

There are several approaches to constrain fault dips with thermochronologic data. The calculation requires knowing: (1) the direction of slip on the fault, (2) the location of at least two temperatures at a particular time (before or during faulting) along the fault trace as defined by FT or other thermochronometers, and (3) either an assumption about the geothermal gradient or a measure of the paleogeothermal gradient from a titled hanging-wall crustal section. The geothermal gradient should be constrained to within about ±10 °C/km for a reasonable estimate of dip (John and Foster 1993; Foster and John 1999; Stockli 2005; Fitzgerald et al. 2009). The variation in paleotemperature along the slip direction of a detachment fault at a particular time is related to the dip of the fault provided that: (1) lateral variations in the thermal gradient (due to voluminous intrusions or hydrothermal flow in the footwall) can be ruled out, and (2) that the samples are from below a single fault system. The second may introduce uncertainty for detachment systems with secondary breakaway faults that result in greater extension in down-dip section.

11.9 Chemehuevi Detachment Example to Constrain Fault Dip

FT and $^{40}Ar/^{39}Ar$ data from rocks in the footwall of the Chemehuevi detachment in Southeastern California constrain the initiation angle of this regional detachment fault system (Foster et al. 1990; John and Foster 1993; Foster and John 1999). Contoured values of mineral cooling age from biotite ($^{40}Ar/^{39}Ar$), K-feldspar ($^{40}Ar/^{39}Ar$), ZFT, AFT, and titanite FT decrease north eastward in the slip direction and define the locations of paleoisotherms in the footwall before and during extension (Fig. 11.5). These thermochronologic data indicate a moderate paleotemperature field gradient across the footwall prior to faulting.

At ~22 Ma, granitic rocks exposed in the southwestern and northeastern portions of the footwall were at ≤200 and ≥400 °C, respectively, and were separated by a distance of some 23 km along the known slip direction. This gradual increase in temperature with depth is attributed to the gentle warping of originally subhorizontal isothermal surfaces and constrains the exposed part of the Chemehuevi detachment fault to have had an initial dip of 15° to 30° using a range of geothermal gradients (Fig. 11.6). Syn-extensional plutons are not present in the southern part of the footwall, so the smooth gradient in paleotemperature is not likely to be due to local variations in the geotherm.

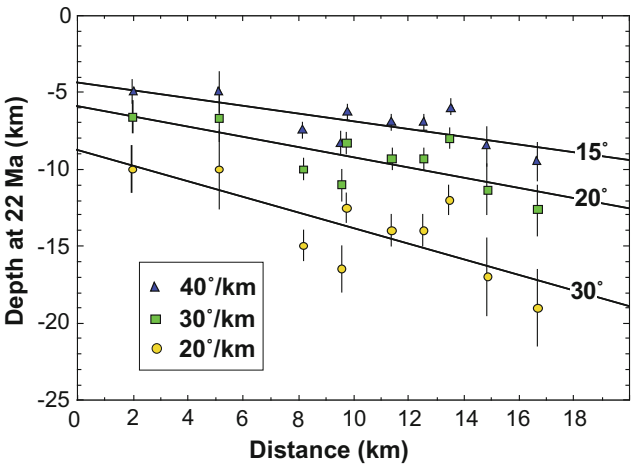

Fig. 11.6 Plot of calculated paleodepth for samples from the southern Chemehuevi Mountains projected to a southwest–northeast cross-section in the direction of slip on the Chemehuevi detachment fault. Paleodepth for each point is calculated from the temperature of each sample at 22 Ma, based on the thermochronologic data assuming three different geothermal gradients. Lines indicate regressions of the data for each gradient and give regional average initial dips of the Chemehuevi detachment

11.10 Conclusions

Many other excellent examples of applications of FT data to structural geology and tectonics exist in the literature. The examples summarized in this chapter provide a general outline for using FT data in normal fault studies. In all cases, a relatively large data set is needed to reduce uncertainty and some of the more powerful applications combine FT, (U-Th)/He, and/or $^{40}Ar/^{39}Ar$ data from the same samples or from the same structure.

Acknowledgements I would like to thank Stephanie Brichau and Paul Fitzgerald for helpful reviews of the original manuscript and the many collaborators that contributed to the studies summarized in this chapter.

References

Bernet M (2009) A field-based estimate of the zircon fission-track closure temperature. Chem Geol 259:181–189

Brichau S, Ring U, Ketcham RA, Carter A, Stockli D, Brunel M (2006) Constraining the long-term evolution of the slip rate for a major extensional fault system in the central Aegean, Greece, using thermochronology. Earth Planet Sci Lett 241:293–306

Brandon MT, Roden-Tice MK, Garver JI (1998) Late Cenozoic exhumation of the Cascadia accretionary wedge in the Olympic Mountains, NW Washington State. Geol Soc Amer Bull 110:985–1009

Brown RW (1991) Backstacking apatite fission-track "stratigraphy": a method for resolving the erosional and isostatic rebound components of tectonic uplift histories. Geology 19:74–77

Brown RW, Summerfield MA, Gleadow AJW (1994) Apatite fission track analysis: its potential for the estimation of denudation rates and implications for models of long-term landscape development. In: Kirkby MJ (ed) Process models and theoretical geomorphology. Wiley, New York, pp 23–53

Campbell-Stone E, John BE, Foster DA, Geissman JW, Livaccari RF (2000) Mechanisms for accommodation of Miocene extension, low-angle normal faulting, magmatism, and secondary breakaway faulting in the southern Sacramento Mountains, southeastern California. Tectonics 19:566–587

Carter TJ, Kohn BP, Foster DA, Gleadow AJW (2004) How the Harcuvar Mountains metamorphic core complex became cool: evidence from apatite (U-Th)/He thermochronometry. Geology 32:985–988

Carter TJ, Kohn BP, Foster DA, Gleadow AJW, Woodhead JD (2006) Late-stage evolution of the Chemehuevi and Sacramento detachment faults from apatite (U-Th)/He thermochronology—evidence for mid-Miocene accelerated slip. Geol Soc Am Bull 118:689–709

Dickinson WR (1991) Tectonic setting of faulted tertiary strata associated with the Catalina core complex in southern Arizona. Geol Soc Am Sp Paper 264

Dumitru TA, Gans PB, Foster DA, Miller EL (1991) Refrigeration of the western Cordilleran lithosphere during Laramide shallow-angle subduction. Geology 19:1145–1148

Ehlers TA, Armstrong PA, Chapman DS (2001) Normal fault thermal regimes and the interpretation of low-temperature thermochronometers. Phys Earth Planet Int 126:179–194

Ehlers TA, Willett SD, Armstrong PA, Chapman DS (2003) Exhumation of the central Wasatch Mountains, Utah: 2. thermokinematic model of exhumation, erosion, and thermochronometer interpretation. J Geophys Res 108(B3):2173

Espurt N, Barbarand J, Roddaz M, Brusset S, Baby P, Saillard M, Hermoza W (2011) A scenario for late Neogene Andean shortening transfer in the Camisea Subandean zone (Peru, 12°S): implications for growth of the northern Andean Plateau. Geol Soc Am Bull 123:2050–2068

Fitzgerald PG (1992) The Transantarctic Mountains of southern Victoria Land: the application of apatite fission track analysis to a rift shoulder uplift. Tectonics 11:634–662

Fitzgerald PG, Malusà MG (2018) Chapter 9. Concept of the exhumed partial annealing (retention) zone and age-elevation profiles in thermochronology. In: Malusà MG, Fitzgerald PG (eds) Fission-track thermochronology and its application to geology. Springer

Fitzgerald PG, Fryxel JE, Wernicke BP (1991) Miocene crustal extension and uplift in southeastern Nevada: constraints from apatite fission track analysis. Geology 19:1013–1016

Fitzgerald PG, Reynolds SJ, Stump E, Foster DA, Gleadow AJW (1993) Thermochronologic evidence for timing of denudation and rate of crustal extension of the South Mountain metamorphic core complex and Sierra Estrella, Arizona. Nucl Tracks 21:555–563

Fitzgerald PG, Duebendorfer EM, Faulds JE, O'Sullivan P (2009) South virgin—white hills detachment fault system of SE Nevada and NW Arizona: applying apatite fission track thermochronology to constrain the tectonic evolution of a major continental detachment system. Tectonics 28 TC2001

Foster DA, Gleadow AJW (1992) The morphotectonic evolution of rift-margin mountains in central Kenya: constraints from apatite fission-track thermochronology. Earth Planet Sci Lett 113:157–171

Foster DA, Gleadow AJW (1993) Episodic denudation in East Africa: a legacy of intracontinental tectonism. Geophys Res Lett 20:2395–2398

Foster DA, Gleadow AJW (1996) Structural framework and denudation history of the flanks of the Kenya and Anza rifts, East Africa. Tectonics 15:258–271

Foster DA, John BE (1999) Quantifying tectonic exhumation in an extensional orogen with thermochronology: examples from the southern Basin and Range Province. Geol Soc (London) Sp Pub 154:356–378

Foster DA, Raza A (2002) Low-temperature thermochronological record of exhumation of the Bitterroot metamorphic core complex, northern Cordilleran Orogen. Tectonophysics 349:23–36

Foster DA, Harrison TM, Miller CF, Howard KA (1990) The $^{40}Ar/^{39}Ar$ thermochronology of the eastern Mojave Desert, California and adjacent western Arizona with implications for the evolution of metamorphic core complexes. J Geophys Res 95:20, 005–20, 024

Foster DA, Miller DS, Miller CF (1991) Tertiary extension in the Old Woman Mountains area, California: evidence from apatite fission track analysis. Tectonics 10:875–886

Foster DA, Gleadow AJW, Reynolds SJ, Fitzgerald PG (1993) The denudation of metamorphic core complexes and the reconstruction of the Transition Zone, west-central Arizona: constraints from apatite fission-track thermochronology. J Geophys Res 98:2167–2185

Foster DA, Grice WC, Kalakay TJ (2010) Extension of the Anaconda metamorphic core complex: $^{40}Ar/^{39}Ar$ thermochronology with implications for Eocene tectonics of the northern Rocky Mountains and the Boulder batholith. Lithosphere 2:232–246

Gleadow AJW, Fitzgerald PG (1987) Uplift history and structure of the Transantarctic Mountains: new evidence from fission track dating of basement apatites in the Dry Valleys area, southern Victoria Land. Earth Plan Sci Lett 82:1–14

Howard KA (1991) Intrusion of horizontal dikes: tectonic significance of Middle Proterozoic diabase sheets widespread in the upper crust throughout the southwestern US. J Geophys Res 96:12461–12478

Howard KA, Foster DA (1996) Thermal and unroofing history of a thick, tilted Basin and Range crustal section, Tortilla Mountains, Arizona. J Geophys Res 101:511–522

John BE, Foster DA (1993) Structural and thermal constraints on the initiation angle of detachment faulting in the southern Basin and Range: the Chemehuevi Mountains case study. Geol Soc Am Bull 105:1091–1108

Karlstrom KE, Heizler M, Quigley MC (2010) Structure and $^{40}Ar/^{39}Ar$ K-feldspar thermal history of the Gold Butte block: reevaluation of the tilted crustal section model. Geol Soc Am Special Paper 463:331–352

Ketcham RA (1996) Thermal models of core-complex evolution in Arizona and New Guinea: implications for ancient cooling paths and present-day heat flow. Tectonics 15:933–951

Lee J (1995) Rapid uplift and rotation of mylonitic rocks from beneath a detachment fault: insights from potassium feldspar $^{40}Ar/^{39}Ar$ thermochronology, northern Snake Range, Nevada. Tectonics 14:54–77

Lister GS, Davis GA (1989) The origin of metamorphic core complexes and detachment faults formed during Tertiary continental extension in the Colorado River region, U.S.A. J Struct Geol 11:65–93

Malusà MG, Fitzgerald PG (2018) Chapter 8. From cooling to exhumation: setting the reference frame for the interpretation of thermocronologic data. In: Malusà MG, Fitzgerald PG (eds) Fission-track thermochronology and its application to geology. Springer

Malusà MG, Fitzgerald PG (2018) Chapter 10. Application of thermochronology to geologic problems: bedrock and detrital approaches. In: Malusà MG, Fitzgerald PG (eds) Fission-track thermochronology and its application to geology. Springer

McQuarrie N, Barns JB, Ehlers TA (2008) Geometric, kinematic, and erosional history of the central Andean Plateau, Bolivia (15–17°S). Tectonics 27 TC3007

Metcalf JR, Fitzgerald PG, Baldwin SL, Muñoz J-A (2009) Thermochronology of a convergent orogen: constraints on the timing of thrust faulting and subsequent exhumation of the Maladeta Pluton in the Central Pyrenean Axial Zone. Earth Plan Sci Lett 287:488–503

Mora A, Ketcham RA, Higuera-Diaz IC, Bookhagen B, Jimenez L, Rubiano J (2014) Formation of passive-roof duplexes in the Colombian Subandes and Peru. Lithosphere 6:456–472

Morrison J, Anderson JL (1998) Footwall refrigeration along a detachment fault: implications for thermal evolution of core complexes. Science 279:63–66

Noble W, Foster D, Gleadow A (1997) The post-Pan-African thermal and extensional history of crystalline basement rocks in eastern Tanzania. Tectonophysics 275:331–350

O'Sullivan PB, Green PF, Bergman SC, Decker J, Duddy IR, Gleadow AJW, Turner DL (1993) Multiple phases of Tertiary uplift and erosion in the National Wildlife Refuge, Alaska, revealed by apatite fission track analysis. AAPG Bull 77:359–385

Pease V, Foster D, O'Sullivan P, Wooden J, Argent J, Fanning C (1999) The Northern Sacramento Mountains, Part II: Exhumation history and detachment faulting. In: Mac Niocaill C, Ryan PD (eds) Continental Tectonics. Geol Soc (London) Sp Pub 164:199–237

Reiners PW, Brady R, Farley KA, Fryxell JE, Wernicke B, Lux D (2000) Helium and argon thermochronometry of the gold butte block, south Virgin Mountains, Nevada. Earth Planet Sci Lett 178:315–326

Spiegel C, Kohn BP, Belton DX, Gleadow AJW (2007) Morphotectonic evolution of the central Kenya rift flanks: implications for late Cenozoic environmental change in East Africa. Geology 35:427–430

Scott RJ, Foster DA, Lister GS (1998) Tectonic implications of rapid cooling of denuded lower plate rocks from the Buckskin-Rawhide metamorphic core complex, west-central Arizona. Geol Soc Am Bull 110:588–614

Singleton JS, Stockli DF, Gans PB, Prior MG (2014) Timing, rate, and magnitude of slip on the Buckskin-Rawhide detachment fault, west central Arizona. Tectonics 33:1596–1615

Spencer JE, Reynolds SJ (1991) Tectonics of mid-Tertiary extension along a transect through west-central Arizona. Tectonics 10:1204–1221

Stockli DF, Dumitru TA, McWilliams MO, Farley KA (2003) Cenozoic tectonic evolution of the White Mountains, California and Nevada. Geol Soc Am Bull 115:788–816

Stockli DF (2005) Application of low-temperature thermochronometry to extensional tectonic settings. In: Reiners PW, Ehlers TA (eds) Low-temperature thermochronology: techniques, interpretations, and applications. Rev Min Geochem 58:411–448. Mineralogical Society of America, Chantilly, Virginia

Stockli DF, Brichau S, Dewane TJ, Hager C, Schroeder J (2006) Dynamics of large-magnitude extension in the Whipple Mountains metamorphic core complex. Geochim Cosmochim Acta 70:A616

Torres Acosta V, Bande A, Sobel ER, Parra M, Schildgen TF, Stuart F, Strecker MR (2015) Cenozoic extension in the Kenya Rift from low-temperature thermochronology: links to diachronous spatiotemporal evolution of rifting in East Africa. Tectonics 34:2367–2386

York D (1969) Least-squares fitting of a straight line with correlated errors. Earth Planet Sci Lett 5:320–324

Wagner GA, Reimer GM (1972) Fission track tectonics: the tectonic interpretation of fission track apatite ages. Earth Planet Sci Lett 14:263–268

Wells ML, Snee LW, Blythe AE (2000) Dating of major normal fault systems using thermochronology: an example from the Raft River detachment, Basin and Range, western United States. J Geophys Res 105:16, 303–16, 327

Wernicke B (1995) Low-angle normal faults and seismicity: a review. J Geophys Res 100:20159–20174

Wernicke B, Axen G (1988) On the role of isotasy in the evolution of normal fault systems. Geology 16:848–851